Mechanism of electron-beam doping in semiconductors

Takao Wada
Department of Applied Electronics, Daido Institute of Technology, 2-21 Daido-cho, Minami-ku, Nagoya 457, Japan

Kyoichiro Yasuda
National Industrial Research Institute of Nagoya, 1-1 Hirate-cho, Kita-ku, Nagoya 462, Japan
(Received 31 May 1995; revised manuscript received 10 October 1995)

A mechanism of electron-beam doping (EBD) was investigated. A semiconductor surface was covered by an overlayer of impurity sheet and the overlayer surface was irradiated with high-energy electrons. Interstitials of displaced atoms in the overlayer, which were introduced by irradiation, migrated to the surface or the interface of the semiconductor. These strongly diffused at the surface with a very large surface diffusivity of the order of 10^{-5} cm^2 sec^{-1} and also had a volume diffusivity of the order of 10^{-15} cm^2 sec^{-1}. High impurity concentrations in the surface layer during irradiation were found to be on the order of the concentration of the matrix atoms. The three main points noted in EBD were the following: (i) there was room-temperature diffusion, (ii) surface diffusion played an important role, and (iii) enhanced diffusions, due to the kick-out mechanism and recombination, occurred.

I. INTRODUCTION

Electron-beam irradiation has mainly been used in order to study damage defects.[1] The threshold for displacement of the sulfur atom from a lattice point in CdS has been measured to be 8.7 eV.[2] In these experiments the crystal was half coated with vacuum-evaporated sulfur 6.8 μg/cm^2 thick. The crystal was bombarded with 100-keV electrons at -100 °C for about 2.3 μA h/cm^2. After irradiation the crystal fluoresced bright green at 77 K under UV stimulation. Myer reported on an electron-beam plasma-doping process in 1971.[3] In the case of these experiments, *n*-type silicon was loosely covered with soft aluminum foil, ~18 μm thick. Using an electron-beam welder, a 10-msec pulse of 100 keV, 0.5 mA and 0.4-mm diameter was aimed at this foil, perforating and volatilizing the foil and forming a miniature plasma at the point of impact. The plasma, in turn, locally melts the underlying semiconductor crystal and injects dopant into the micropuddle thus formed.[3]

In 1980, an electron-beam doping (EBD) method at room temperature was proposed by one of the authors (Wada).[4–11] This study was also concerned with general problems of semiconductor physics. In this method the surface of semiconductor substrates is covered with an overlayer of impurity sheets, which were separated. The surface of the impurity sheet on the substrate is bombarded with high-energy electrons. The electron energy is 750 keV and 3–9 MeV, and the electron fluence is $(1–10)\times10^{17}$ e cm^{-2}. More effective EBD is obtained in another case of a two-layer system in which the impurity layers were deposited on the substrate. Alloying layers are also formed at the interface of such samples.[12] If water is used instead of an impurity sheet, EB oxide layers are grown on the substrate.[13] The mechanism of EBD, however, has not been clear. Surface diffusion of impurity atoms is an interesting process, but there has been little study of it.

In the present paper, we carried out experiments on the surface diffusion of impurities, and on the electron energy dependences of the impurity concentrations for samples of a two-layer structure such as Ge/Si (the Ge wafer is placed on top of Si crystals) and Zn/GaAs by electron-beam doping. The latter is compared with calculations of the concentration for the displaced atoms done on the basis of classical Coulomb scattering. The energy spectra of primary displaced atoms were calculated from the electron energy spectra estimated by means of a Monte Carlo simulation. The mechanism of EBD was experimentally and theoretically investigated, taking account of migrations of interstitial atoms, surface diffusion, the surface layer of high concentration impurities, and the concentration- and recombination-enhanced diffusions.

EBD processes would be useful with advantages over alternative doping techniques, because even in the damageless region and at room temperature doping processes may be possible.

II. EXPERIMENTAL PROCEDURES

The wafers used in the experiments for temperature dependences of EBD were *p*-Si [B-doped (111), 25–50 Ω cm, $5\times5\times0.35$ mm^3] and *n*-Ge [Sb-doped (111), $5\times5\times0.5$ mm^3] [Fig. 1(a) (i)].

For the experiment of surface diffusion using the sample of Ge/Si, a surface of Si substrate [*n*-type, N-doped (111), $\rho=20–45$ Ω cm, $17\times30\times0.25$ mm^3] after RCA cleaning was covered partially with a Ge wafer [*n*-type, Sb-doped (111), $\rho=0.01$ Ω cm, $10\times10\times0.5$ mm^3], as shown in Fig. 1(a) (ii). The overlain sheets are in physical contact with the substrate, whose surface has a surface microroughness within about 10 Å. Only the surface of the Ge wafer was irradiated locally through an aperture of thick Al plate over the sample in a vacuum (10^{-5} Torr), and with a total fluence of 1×10^{18} e cm^{-2} at 7 MeV from an electron linear accelerator as shown in Figs. 1(a) (iii) and 1(b). The thickness of 40–50 mm for the Al plate is much larger than the range (~15 mm) of electrons. The edge of the aperture of the Al plate was aligned with the edge of the Ge wafer on the Si substrate,

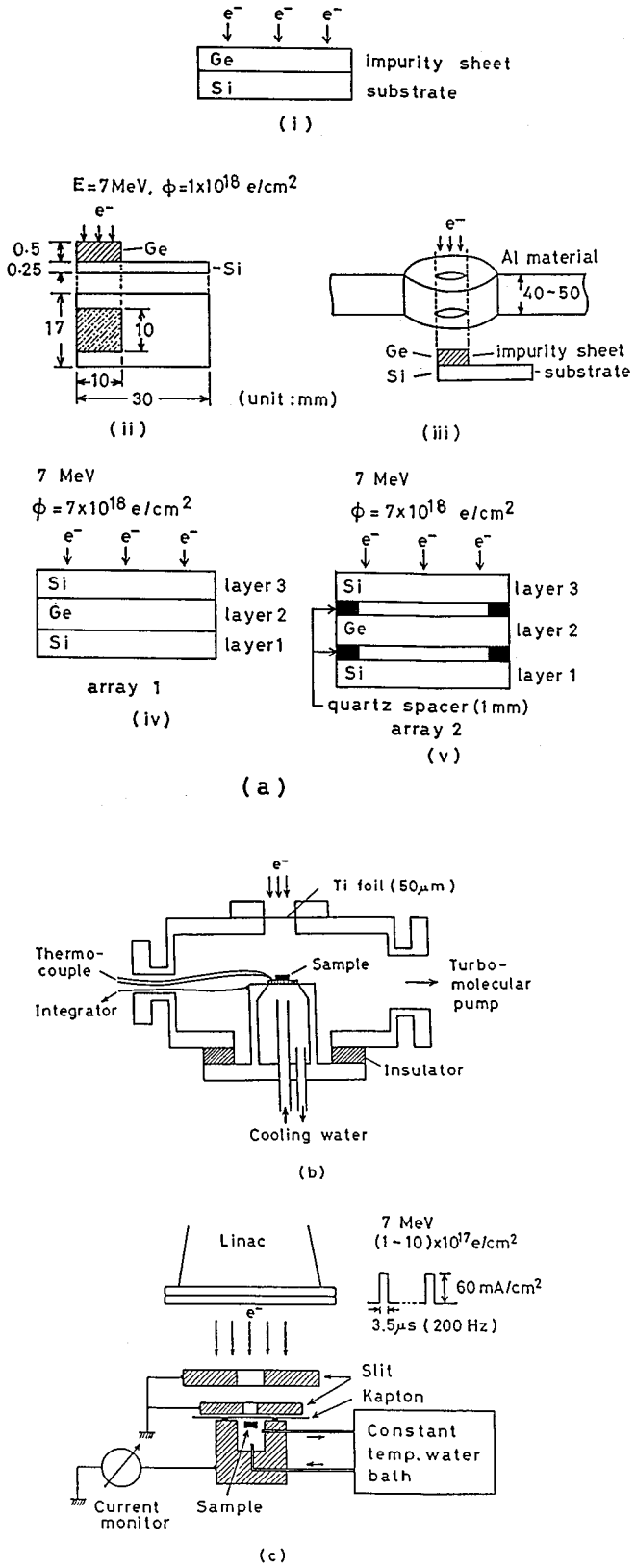

FIG. 1. (a) Schematic diagram of EBD experiments for the temperature dependences (i). For the surface diffusion in vacuum for the sample dimension (ii), thick Al materials used to mask perfectly (iii), and for the effect of interface between substrates and overlain sheet [(iv) and (v)]. Schematic diagrams of electron irradiation in vacuum (b) and in water (c).

such that only the overlayers were irradiated. The accelerator operated with a pulse width of ~ 3.5 μs, a 200-Hz duty cycle, and an average electron-beam current of 40 μA cm^{-2} (a peak current density of 60 mA cm^{-2}). In this case, the temperature was about 150 °C, which was monitored by a thermocouple contacting the sample. After irradiation and RCA cleaning, the concentration profiles of impurity atoms in Si were measured utilizing secondary-ion-mass spectroscopy (SIMS) (CAMECA IMS-3f). A focused oxygen ion beam (diameter ~ 40 μm) with an ion energy of 8 keV was used in a 5×10^{-9}-Torr vacuum.

For experiments on the electron energy dependence of the impurity concentration, the samples of the two-layer structure Ge/Si, which was composed of a Ge overlayer [Sb-doped (111), $5\times5\times0.5$ mm^3] and a Si substrate [B-doped (111), 25–50 Ω cm, $5\times5\times0.35$ mm^3], were irradiated with a total fluence of $\sim 5\times10^{17}$ e cm^{-2} at 3, 5, and 7 MeV. The samples were enveloped by an Al foil. This foil was supported in a gap between a kapton foil and a mount, and was put in a circulating water bath. The bath was kept at a constant temperature of 60 °C by using a thermoregulator, as shown in Fig. 1(c). The beam heat transfer was done from the samples to the chamber walls of copper (or stainless steel), or the water and then onto the substrate. Distributions of Ge impurity atoms in Si were measured by SIMS and a Rutherford backscattering spectrometer (RBS). The values measured by SIMS were in agreement with those done by RBS.

The two-layer structures of the Zn overlayer and GaAs substrate, Zn/GaAs, were also used. Wafers of the substrate were (100)-oriented Si-doped GaAs (t=0.5 mm), and the Zn materials were 99.99% pure sheet with dimensions of $6\times6\times0.2$ mm^3. t represents the thickness of the wafers. The surface of the overlayers was irradiated with a total fluence of 1×10^{17} e cm^{-2} at 7 MeV and at 50 °C in water from the electron linear accelerator, and 2×10^{17} e cm^{-2} at 750 keV and at 100 °C in air, with a mean current density of 8.1 μA cm^{-2} from the Van de Graaf accelerator provided by Nissin-High Voltage Co. Ltd.

In the experiments for atoms crossing the gap and interface to the substrate, a Ge wafer was sandwiched between two Si wafers in an array 1 [Fig. 1(a) (iv)], and was placed with separations of 1 mm between Si wafers in an array 2 in which quartz pieces [$1(t)\times2\times2$ mm^3] were used as spacers [Fig. 1(a) (v)]. Spacers were set in corners on wafers of layers 1 and 2, as shown in the figure.

In the three-layer systems, the Zn sheet was sandwiched between Si and GaAs, and each was in contact with another surface; that is, Si (layer 3)/Zn (layer 2)/GaAs (layer 1). Their samples were (100)-oriented undoped semi-insulating GaAs ($t\simeq0.6$ mm) grown by liquid-encapsulated Czochralski (LEC), (100)-oriented B doped p-type Si ($t\simeq0.5$ mm) and 99.9% Zn ($t\simeq0.5$ mm). The surface of layer 3 was irradiated with a fluence of $\sim 5\times10^{17}$ e cm^{-2} at 7 MeV and 50 °C. Photoluminescence (PL) measurements were also performed at 77 K. The samples were immersed in liquid nitrogen, and a focused argon laser beam (80 mW, 5145 Å) was used as the excitation source.

III. EXPERIMENTAL RESULTS

A. Temperature dependence of EBD

There exists the following proof that EBD is not a thermal process. In the case of a Ge overlain sheet ($t\sim0.5$ mm) and

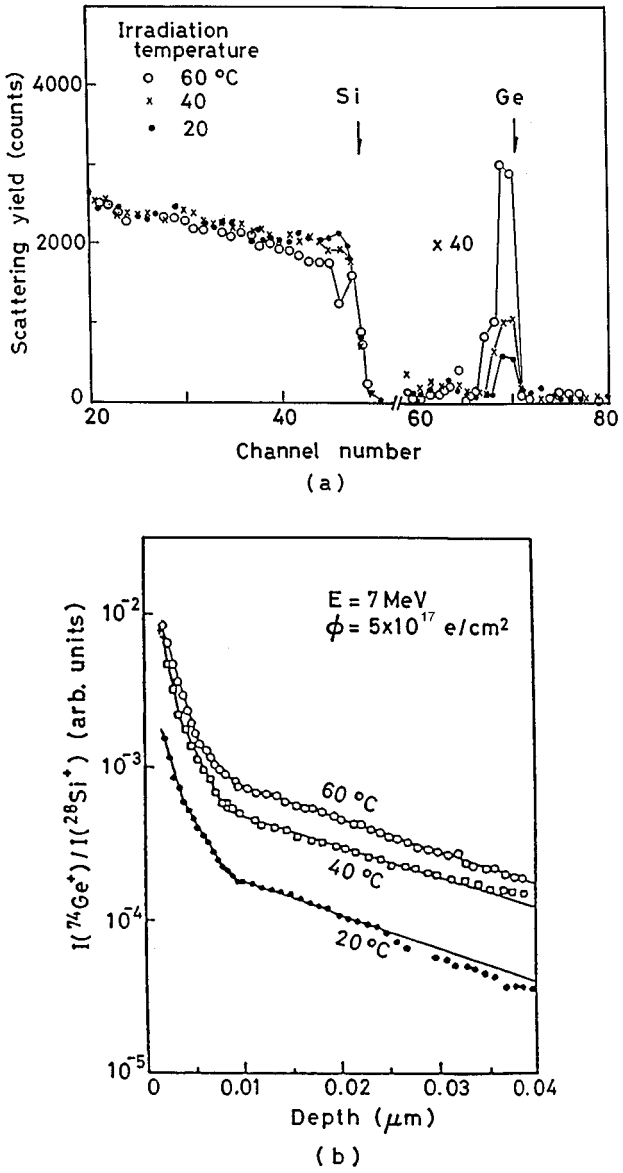

FIG. 2. (a) Backscattering spectra for the irradiated Si at random conditions at different irradiation temperatures. (b) Intensity ratios of $^{74}Ge^{+}$ to $^{28}Si^{+}$ in the Si substrate as a function of depth from the front surface of Si.

Si substrate, the backscattering spectra in random conditions by 1.4-MeV He^{+} ions are shown in Fig. 2(a) for the specimens irradiated at 20, 40, and 60 °C in water with a total fluence of $\sim 5.1\times10^{17}$ e cm^{-2} at 7 MeV. The number of Ge peaks in Si increases with increasing irradiation temperature. From a curve of the maximum Ge concentrations C_{Ge} estimated from the backscattering spectra versus reciprocal irradiation temperature, an activation energy of the sputtering yield for Ge atoms into Si is estimated to be about 0.3 eV. The intensity ratios of $^{74}Ge^{+}$ ions to $^{23}Si^{+}$ ions in the case of Ge ($t\sim0.5$ mm)/Si irradiated by the same conditions as described above are shown in Fig. 2(b) as a function of depth measured from the Si front surface, which is in contact with the overlayer. SIMS measurements were performed by using the primary ion (O_2^{+}) beam with an ion energy of 7 keV. For Si wafers irradiated without impurity sheets, the Ge^{+} peak disappeared.

The diffusion profile is not a complementary error function. This suggests that the diffusivity is concentration dependent. The analyses of Boltzmann[14] and Matano[15] are used to obtain the concentration C dependence of the diffusivity $D(C)$. The values of $D(C)$ at $x<0.01$ μm and $x>0.01$ μm for Ge are observed to be 10^{-18}–10^{-16} and $\sim10^{-16}$–10^{-14} cm^2 sec^{-1}, respectively. These estimated values of diffusivity are much larger than what would usually be expected at 50 °C in a case of a mainly thermal process. The value of C_o is estimated to be $\sim1.4\times10^{20}$ cm^{-3}. The resultant plot is mainly composed of three curves. It is suggested that three kinds of species diffuse into the substrate. The diffusivities of $D(C)$ at $C=1\times10^{20}$ cm^{-3} for 20, 40, and 60 °C which are estimated by the analysis of Boltzmann and Matano from the curves, are indicated as a function of reciprocal irradiation temperature. From this curve, an activation energy for the diffusivity in Si is obtained to be about 0.2 eV. Also, the intensity ratio of $^{74}Ge^{+}$ ions to $^{28}Si^{+}$ ions in the case of the irradiation in a vacuum for Ge ($t\sim0.5$ mm)/Si was measured. The sample was irradiated with a fluence of $\sim4.7\times10^{17}$ e cm^{-2} at $\sim$250 °C. The values of $D(C)$ range from 10^{-18} to 4×10^{-15} cm^2 sec^{-1}. The value of C_o is estimated to be $\sim5\times10^{20}$ cm^{-3}. The concentration profile of impurity atoms in Si irradiated in a vacuum is similar to that irradiated in the water bath. This suggests that interfacial oxides and capillary water layers in the contact of the overlayer and substrate might not be seriously affected for electron-beam doping. It is considered that the displaced impurity atoms may mainly migrate in the interface of overlain wafers and substrates by surface diffusion, as will be cited below, and that very few displacements transfer to the chamber wall or water or to other materials in contact with the overlayer.

B. Surface diffusion

Figure 3(a) shows the concentration profiles of Ge atoms as a function of lateral position x in the unirrradiated regions of the Si substrate surface. It is shown that Ge atoms were detected even at a distance of 10 mm from the edge of the overlayer. It is found that Ge impurities diffused into the unirradiated regions, i.e., that surface diffusion occurs. The parameters are the different depths of 50, 100, and 200 Å from the Si surface. The resultant plot is mainly composed of two curves. This suggests that two kinds of species diffuse at the surface. The diffusivities D_s for the surface diffusion are estimated as $(1.7\text{–}2.9)\times10^{-5}$ cm^2 sec^{-1} from these profiles by using the analysis of Boltzmann and Matano,[16] and they are on the order of 10^{10} times larger than volume diffusivities.

In the similar case of GaSb (n-type, 5×5 mm^2)/Zn/GaSb (n-type, 5×10^{17} Te cm^{-3}, 5×15 mm^2, $t\sim400$ μm) irradiated locally by electron beam as shown in Fig. 3(b), the resistivities of the GaSb substrate were measured by the four-point probe method. These results show that only the irradiated region became a high resistivity layer, and that the unirradiated region ($x>6$ mm) did not change from the original resistivity. This suggests that the region of substrates which is not covered by the overlayer, as shown in Fig. 1(a) (ii), is not irradiated. The electron beam may have scattered sideways within several tens μm out of the edges of the Ge sheet to produce the observed doping, as mentioned in a previous paper.[17]

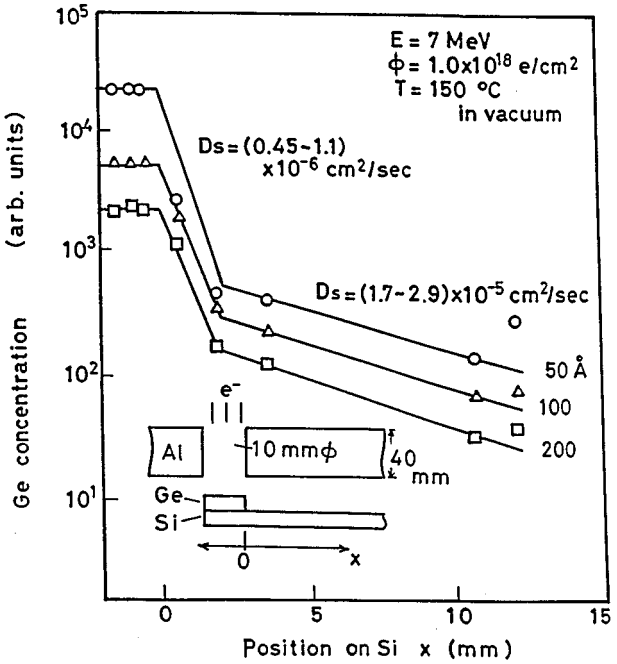

(a)

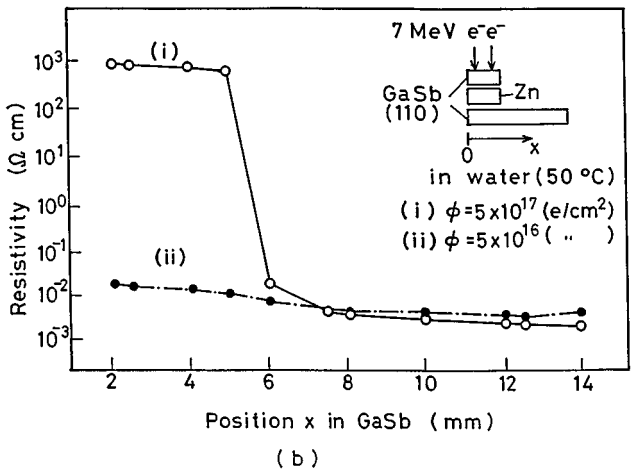

(b)

FIG. 3. (a) Concentration profiles of Ge atoms which were introduced into the Si substrate as a function of the lateral position in the unirradiated region, measured at different depths. (b) Resistivity profiles of GaSb substrates (5×15 mm^2) irradiated locally and covered partially by the overlayers of GaSb/Zn(5×5 mm^2) as a function of lateral position in the substrate.

C. Electron energy dependence of impurity concentrations

1. 3-, 5-, and 7-MeV electron irradiations of Ge/Si

The relative signal intensity ratios $I(^{74}\mathrm{Ge})/I(^{28}\mathrm{Si})$ measured by SIMS at the surface of the Si substrate are shown by a mark *o* in Fig. 4 as a function of electron energy. The ratios increase with the increase of electron energy.

2. 0.75- and 7-MeV electron irradiations of Zn/GaAs

Figure 5 shows typical ratios of the SIMS signal intensity of Zn to that of Ga in the GaAs substrate irradiated by 0.75- and 7-MeV electrons as a function of depth from the surface of GaAs. The impurity concentration doped by 7-MeV electrons is about 3.8 times as large as that doped by 0.75-MeV electrons at the surface. The resultant plots are also mainly composed of three curves. The diffusivities obtained from these curves are about 10^{-17} and 10^{-15} cm^2 sec^{-1} at 0.75 MeV, and about 10^{-16} and 10^{-14} cm^2 sec^{-1} at 7 MeV, respectively. The ratios $I(^{64}\mathrm{Zn})/I(^{69}\mathrm{Ga})$ at the surface of the GaAs substrate are shown by a mark ○ in Fig. 6.

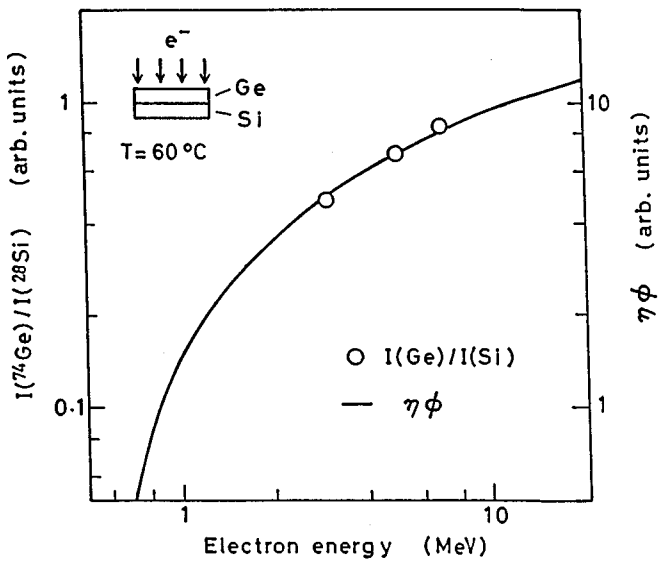

FIG. 4. Electron energy dependences of SIMS intensity ratio $I(^{74}\mathrm{Ge})/I(^{28}\mathrm{Si})$, and theoretical concentration of displaced Ge atoms in a Ge wafer.

D. Three-layer array

The results of SIMS measurements were plotted in arbitrary units as functions of depth from the front and back

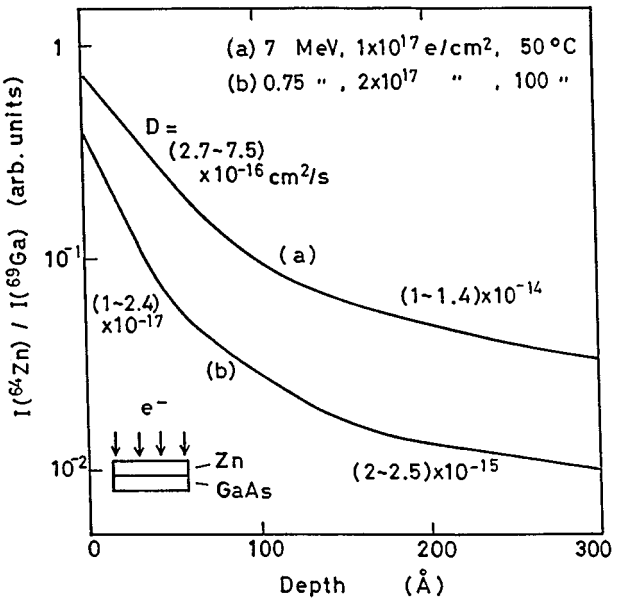

FIG. 5. SIMS intensity ratios of $I(^{64}\mathrm{Zn})/I(^{69}\mathrm{Ga})$ as a function of depth in the GaAs substrate for the samples of Zn/GaAs irradiated with 1×10^{17} e/cm^2 at 7 MeV and 2×10^{17} e/cm^2 at 0.75 MeV.

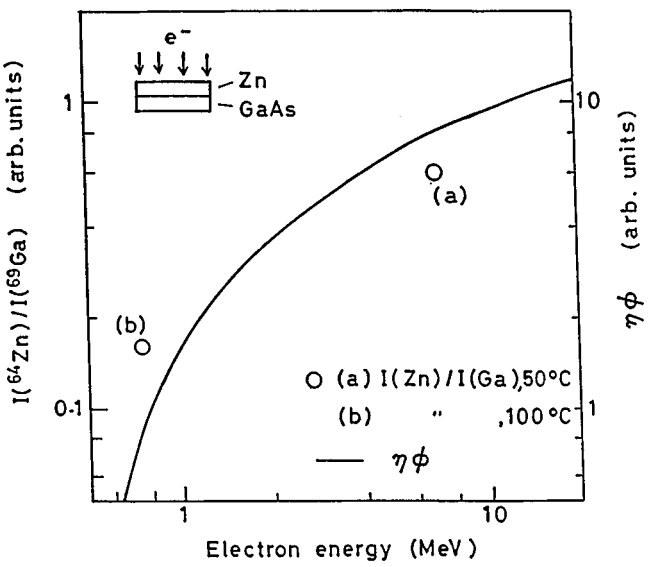

FIG. 6. Electron energy dependences of SIMS intensity ratios $I(^{64}\mathrm{Zn})/I(^{69}\mathrm{Ga})$ and theoretical concentration of displaced Zn atoms in a Zn sheet.

surfaces. The concentration profiles of Zn and Si atoms in a GaAs wafer are shown in Fig. 7. Surprisingly, the results indicate that the irradiation caused not only the indiffusion of Zn atoms from layer 2 (Zn), but also that of Si atoms from layer 3 (Si) into layer 1 (GaAs) through layer 2 (Zn). The concentrations of both Zn and Si atoms are very high near the surface, while they seem relatively low and almost constant except in the vicinity of the surface; i.e., the profiles are *U* shaped. The diffusivities *D* estimated from the SIMS profiles using the analysis of Boltzmann and Matano are also indicated in the figure for both Zn and Si atoms.

Figure 8 shows a typical result of the PL measurement. The PL spectrum at 77 K from the front surface of GaAs

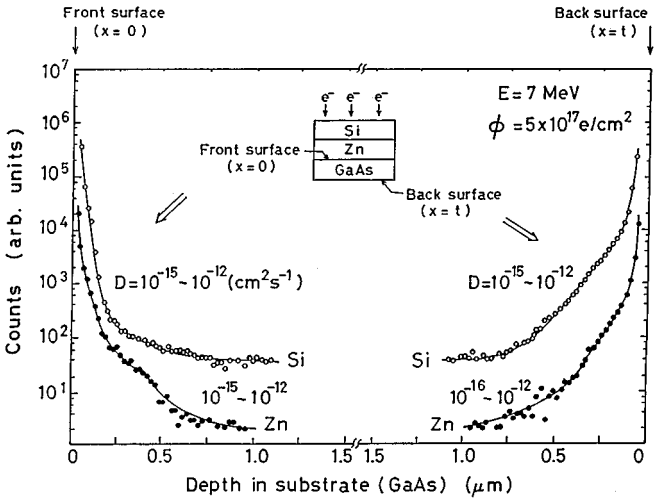

FIG. 7. Concentration profiles of Zn and Si atoms in GaAs (layer 1) measured by SIMS as functions of depth from both the front and back surfaces. Values of the diffusivity *D* are also indicated in $\mathrm{cm}^2\ \mathrm{s}^{-1}$.

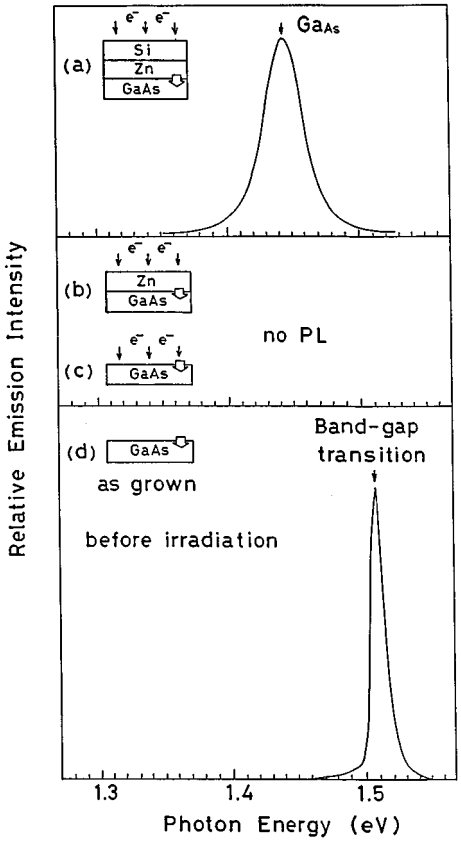

FIG. 8. 77K-PL spectrum for a GaAs wafer of the sandwiched array of Si/Zn/GaAs (array III) (a), array of overlayer Zn/substrate GaAs (array II) (b), and without a Zn sheet (c). 77K-PL spectrum for a typical virgin GaAs specimen before irradiation (d). The measurements were all done before thermal treatment.

(layer 1) consists of a single peak even before annealing, as shown in Fig. 8(a). The peak at 1.44 eV with a full width at half maximum (FWHM) of 0.035 eV is attributed to the Ga antisite defect, $\mathrm{Ga}_{\mathrm{As}}$.[18–20] The result of PL measurement from the back surface of layer 1 is similar to that shown in Fig. 8(a). However, although the GaAs wafer before irradiation initially shows strong band-edge emission [see Fig. 8(d)], no PL observed from the GaAs substrate before annealing when the GaAs wafer was irradiated ($E=7$ MeV, and $\Phi=5\times10^{17}\ e\ \mathrm{cm}^{-2}$) without a Zn sheet[21] [see Fig. 8(c)], or when it was irradiated in a two-layer array of Zn/GaAs [see Fig. 8(b)].

E. Effect of interface between substrates and overlain sheet

Three-layer structures (arrays 1 and 2) are illustrated schematically in the insets of Figs. 9(a) and 9(b). Surfaces of overlayers (Si of layer 3 in the respective array) were irradiated with a total fluence of $7\times10^{18}\ e\ \mathrm{cm}^{-2}$ at 7 MeV from an electron linear accelerator. During irradiation, samples were kept in a vacuum of 10^{-5} Pa and at about 50 °C.

Figure 9(a) shows the Auger electron spectroscopy (AES) energy spectra obtained from a front surface of Si (layer 1), whose direction is indicated by an arrow in the inset of the figure. The signal intensity of Ge *LMM* is nearly equal to that of Si *KLL*. This means that a number of Ge atoms are ad-

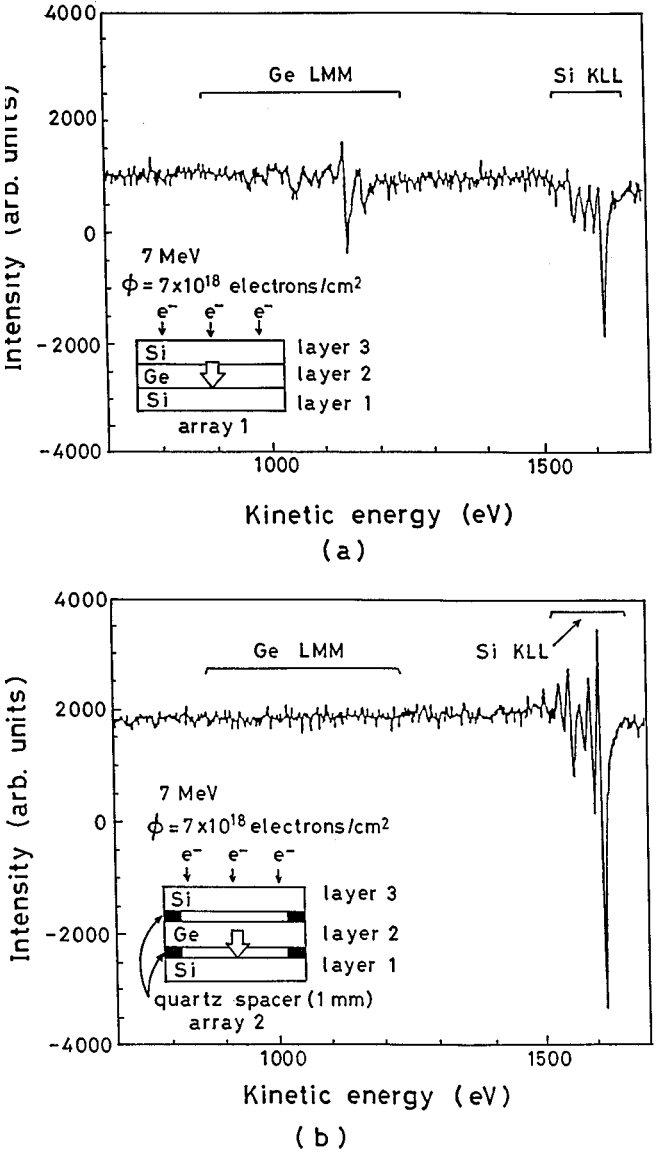

FIG. 9. AES spectra obtained from the surface of Si (layer 1) in array 1 (a) and array 2 (b), which are indicated by an arrow, respectively.

sorbed at the Si surface. The AES signal of Ge was also observed from the Si surface of layer 3. Si atoms were also detected from the both surfaces of the Ge sheet by AES. Figure 9(b) shows the AES spectra obtained from the Si surface, whose direction is indicated by an arrow in an array 2 in the inset of the figure. No Ge signal can be observed. On the surface of the other Si wafer (layer 3) and both surfaces of Ge sheet, Ge and Si atoms could not be detected by AES. In this experiment, as the displaced atom did not diffuse through a surface of insulating quartz spacers,[22] Ge atoms of layer 2 could not arrive the surface of the Si wafer (layer 1).

The latter results suggest that the displaced atoms in the overlayer can scarcely be emitted into the vacuum, and hardly be adsorbed on the substrate wafers. Therefore EBD can be performed only when the overlayer is in contact with the surface of the substrate, because of the occurrence of surface diffusion of atoms at the interface of contacted wafers.

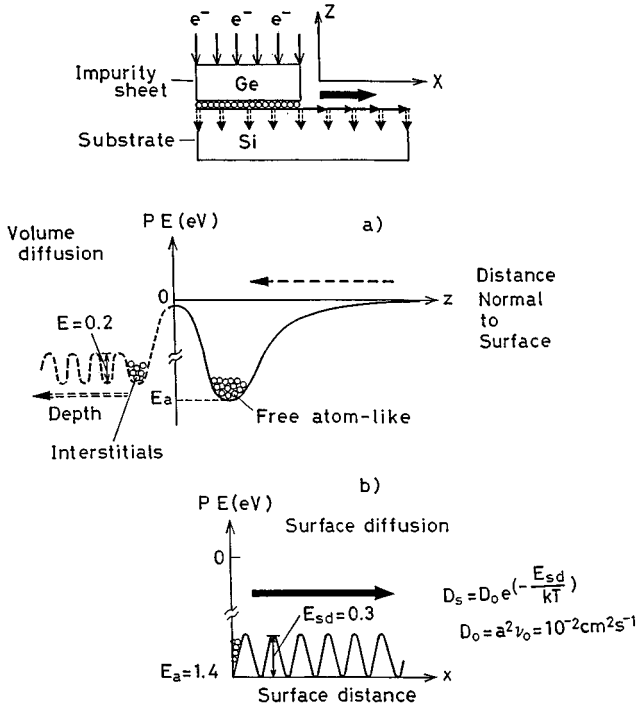

FIG. 10. (a) Potential energy of adsorbed atoms as a function of distance normal to surface and migration into the substrate (upper), and (b) the surface diffusion parallel to the surface of the substrate (lower).

IV. DISCUSSION

A. Factors (D_s, X_s, τ, E_a, and E_{sd}) in surface diffusion

Surface diffusion of impurity atoms is the most interesting point. Figures 10(a) and 10(b) show schematic views of the potential-energy distribution at or near the surface. The diffusion length of surface diffusion X_x is given by

$$X_s^2 = D_s \tau_a , \tag{1}$$

where D_s is the diffusivity of the surface diffusion, and τ_a represents stay times for the adsorption, which are written by[23]

$$\tau_a = \exp(E_a/kT)/\nu = \tau_0 \exp(E_a/kT), \tag{2}$$

where τ_0 is considered to be the inverse of the adatom vibrational frequency normal to the surface, E_a is an adsorption energy which depends on the degree of surface coverage, and D_s is given by

$$D_s = a^2 \nu_0 \exp(-E_{sd}/kT), \tag{3}$$

where a is lattice constant, and E_{sd} the activation energy of migration of an adsorbed atom. The diffusivities D_s are estimated as 2.3×10^{-5} cm^2 sec^{-1} from the profiles by using the analysis of Boltzmann and Matano[16] in the experiment with Ge/Si. By using the experimental values of D_s and X_s, and assuming $\nu_0 = 10^{13}$ sec^{-1}, τ_a and E_a are roughly estimated as 10^4 sec and 1.4 eV, respectively. These values of τ_a and E_a for the adsorbed atom correspond to those in a loosely bound phase, which have been reported for the adsorption of cadmium on tungsten.[23] For $a^2 \simeq 10^{-15}$ cm^2, $E_{sd} \simeq 0.3$ eV at

TABLE I. Estimated concentrations of Frenkel defects, observed complex defects, measured total vacancy defects, recombination defects and interstitial sinks near the surface. Example of electron irradiation. 0.3 mm(t)$\times 10^{18}$ cm$^{-3}\simeq$100 Å(t)$\times 10^{22}$ cm^{-3}.

	Number
Total fluence of 7 meV electrons	$\phi=4\times10^{18}$ e cm^{-2}
No. of Frenkel defects	N_F=(production rate in Si$\times$ fluence) $=8\times4\times10^{18}=3.2\times10^{19}$ cm^{-3} (100%)
Measurement of defect density	
(1) V (vacancy)+O (Oxygen)	
[A center]	5% (DLTS)
(2) V_2+O	1.5% (EPR)
(3) V_2^- (divacancy)	0.8% (EPR)
(4) I_2^+ (di-interstitial)	0.08% (EPR)
Total observed vacancy defects	$N_{\Sigma V}=N_{V+O}+N_{V2}+N_{v2+O}$ $\simeq 10\%(3.2\times10^{18}$ cm^{-3}
Recombination rate of self-interstitials and vacancies ($I+V\rightarrow$annihilation)	$N_F-N_{\Sigma V}\simeq 90\%$ N_F
Total interstitial density ($\simeq$total vacancy density)	$N_i+N_{i2}=N_{\Sigma V}\simeq 10\%$

150 °C in vacuum for Ge/Si, while for Zn/GaAs $D_s=10^{-4}$ cm^2 sec^{-1}, $\tau=1\times10^3$ sec, $E_a=1.0$ eV, and $E_{sd}=0.1$ eV at 50 °C in water. These mean that an adsorbed atom migrates as a free atom at the surface, because of the very large value of D_s.

Using Pauling's formula[24] for the calculation of E_a based on a covalent bonding model, E_a is given by

$$E_a=\tfrac{1}{2}(D_{AA}+D_{BB})+23.06(\chi_A-\chi_B)^2, \tag{4}$$

where D_{AA} and D_{BB} are the bond energies for like molecules, and χ_A and χ_B are the corresponding electronegativity coefficients. One calculates the case for germanium on silicon as $E_a=1.73$ eV, as opposed to the observed value of $E_a=1.4$ eV. This may depend on the degree of surface coverage.

B. Surface layer of high concentration impurities

A number of vacancy and interstitial pairs as Frenkel defects are produced in a crystal such as Si by irradiation of high-energy electrons. A large fraction of vacancies may recombine with the interstitials. While some part of the vacancies form complex defects such as oxygen-vacancy pairs and impurity atom-vacancy pairs, which result in stable defects, generally surface region is considered as a sink for defects, involving displaced atoms such as interstitials. Unrecombined interstitials migrate and sink at or near the surface.

For simplicity, the production rate η of Frenkel defects in Si for a 7-MeV electron is assumed to be about 8 cm^{-1}.[25] The concentration of Frenkel defects introduced with $\Phi=4\times10^{18}$ e cm^{-2} as $N_F=3.2\times10^{19}$ cm^{-3}, as indicated in Table I. Experimentally the respective values of η for V_2,V_2+O, and V+O complex defects were obtained as 0.8%, 1.5%, and 5%, respectively, as tabulated in Table I. They were measured by electron paramagnetic resonance (EPR) for V_2 and V_2+O, and deep-level transient spectroscopy (DLTS) for V+O. From these results, the total concentration of the vacancies, being stable due to the complex defects as above, is about 10% Frenkel defects ($\sim3.2\times10^{18}$ cm^{-3}) (Table I). A remainder concentration (90%) of vacancies may mainly recombine with the interstitials of Frenkel defects in the bulk of the wafer (Table I). Therefore there are unrecombined interstitial concentrations in crystal, nearly equal to that of the total observed vacancies (10%) (Table I). They may sink at or near the surface. If 10% of the unrecombined interstitials, produced in the overlain wafer with a thickness of 0.03 cm, migrate and sink into the surface layer of 100 Å, the concentration of migrating interstitials becomes on the order of the matrix atoms (Table I). The surface diffusivities of impurities were on the order of 10^{10} times as large as the volume diffusivities.[16] The supersaturation of the introduced interstitial may be built up near the wafer surface, depending on whether the kick-out mechanism dominates.[26] A monolayer or so of impurity atoms at or near the surface of the substrate may possibly be formed during irradiation. An origin of the enhanced diffusion of the impurity into the substrate may be the surface high concentration layer. The experimental results suggested that roughly about 0.1–1% of the total displaced atoms (Frenkel defects) produced in the overlayer by electron irradiation were doped into the substrate.

C. Energy spectra of primary displaced atom

During irradiation, the incident electrons collide with target atoms, transfer part of their energy, and produce primary displaced atoms. The displaced atoms in turn collide with other atoms in the lattice, thereby producing additional displaced atoms (interstitials) and vacancies, i.e., the Frenkel defect. It seems that the energies transferred to the displaced atoms are significant for EBD.

The energy spectra of electrons at different depths in Si for incident electron energies of 0.75 and 7 MeV were calculated. The results were obtained by using Sugiyama's program[27] for a Monte Carlo simulation for the theory of fast electron penetration in matter.[17] The program took account of multiple scattering of electrons, straggling of electron energy losses by ionization and excitation of atoms, production of knock-on electrons, and bremsstrahlung photons. For photon penetration, the photoelectric effect, Compton effect, pair production, and annihilation radiation from positrons at rest or in flight were also taken into consideration. Lattice vibration due to electron irradiation and electron channeling is not considered in the calculation. Although electrons transmitted by electron channeling exhibit an orientation dependence, the effect of this may be small due to the scattering of electrons in the sample with a large thickness. Electron channeling has been measured for the sample with the thickness of ~ 6 μm.[28] The electron energy spectra $n(E_0,E_B,z)$ calculated with this program were in agreement with the experimental results for 400-keV electrons.[17] The energy spectra of primary displaced atoms were calculated from the electron energy spectra as a function of average energy transfer $\overline{E_p}$[29,30]

$$\overline{E_p}=E_d(\ln E_m/E_d-1+\pi\alpha), \tag{5}$$

where $\alpha=Z/137$, and Z is the atomic number of the struck atoms, E_d a characteristic displacement energy, and E_m the maximum energy transfer. E_m is given by

$$E_m(\mathrm{eV})=560.8X(X+2)/A, \tag{6}$$

where A is the atomic mass of the stuck atom. $X=E_B/mc^2$, and $mc^2=0.511$ MeV. The number of primary displaced atoms as a function of average energy transfer and depth $N_p(E_0,\overline{E_p},z)$ is given approximately by

$$N_p(E_0,\overline{E_p},z)=n_0\sigma(E_B)n(E_0,E_B,z)(dE_B/d\overline{E_p}), \tag{7}$$

Figure 11 shows the energy spectra of primary displaced atoms at various depths calculated for the Si sample with a surface area of 4×4 cm^2, and thicknesses of 0.2 and 2 cm irradiated by 0.75- and 7-MeV electron beams with a diameter of 20 μm from the electron energy spectra, respectively. This figure indicates that average energies of around 18 and 108 eV are transferred to the primary displaced atoms near the surface and at $z<0.18$ cm in Si samples for electron energies of 0.75 and 7 MeV, respectively. Experimentally, Al, Zn, and Si atoms were doped into GaAs by EBD methods upon 0.75-MeV electron irradiation. For Ge atoms, the average energy transfer calculated is about 98 eV at the incident surface of the Ge sample upon irradiation of 7-MeV electrons. These energies correspond to those of the evaporated carbon in ion plating on an n-type wafer.[31] It seems that these values of the energy transfer are effective for the production of subsequent displacements (interstitials and vacancies) by recoil and the enhancement of migration of interstitial atoms in the impurity sheet, and also for the migration of interstitials (impurity atoms) due to the concentration-enhanced diffusion into the substrates across the interface.

The beam heat of the EBD sample is estimated as follows. An electron-beam irradiation was carried out with a peak current density of 60 mA/cm^2 (an average current density of 40 μA/cm^2), a pulse width of ~ 3.5 μsec, a 200-Hz duty cycle, on an electron energy of 7 MeV. The samples (two- or three-layer structures) have a dimension of $0.5\times0.5\times(0.06-0.1)$ cm^3. For the above conditions, the absorbed electrical energies in the sample are about 5.4×10^{-3} Cal/pulse (transiently) and 1.1 Cal/sec (steady). Then the rates of the temperature rise are about 0.55 °C/pulse and 110 °C/sec. However, these samples were cooled by placing them in a circulating water bath, which was kept at a constant temperature, and by contacting with the cooled plate of a sample mount in a vacuum. The temperature of sample measured by thermocouple during irradiation were 20–60 °C in water, and 50–150 °C in vacuum. Table II summarizes the energy of displaced atoms calculated from the electron energy spectra in a sample, and the temperature of a sample and the apparent temperature of displaced atoms during EBD experiments. In the EBD process, it is expected that the whole sample was kept at a given (constant) temperature due to the beam heat transfer from the sample to the chamber walls or the water, and that only the displaced atoms have an apparent very high temperature, which corresponds to an energy of struck atom. These primary displaced atoms may have enough energy to produce subsequent displacements, and they may create ones up to less than the threshold energy for atomic displacement, 25 eV after a collision.

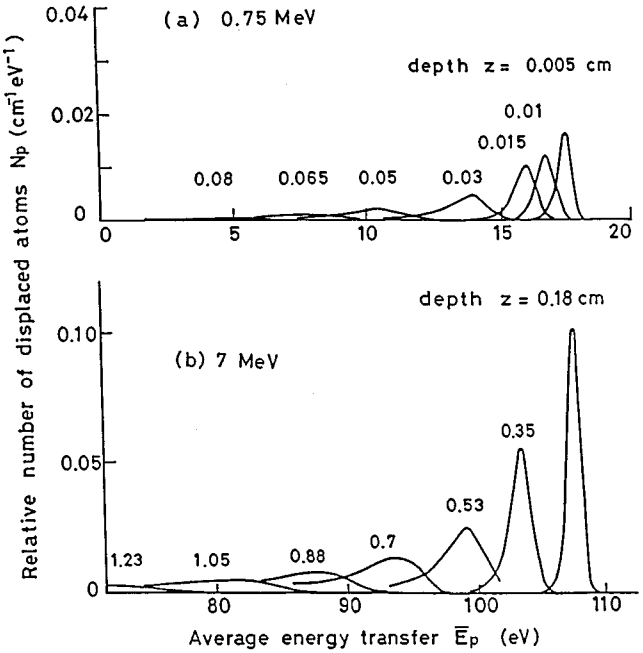

FIG. 11. Theoretical energy spectra of primary displaced atoms as a function of average energy transfer for Si samples irradiated with 0.75- (a) and 7-MeV electrons (b).

D. Electron energy dependence of the impurity concentration

The concentrations of displaced atoms are given by $\eta\Phi$ on the basis of classical Coulomb scattering, where η is the production rate of displaced atoms and Φ electron fluence. η is given by Cahn[25] as follows:

TABLE II. EBD with a fluence of $\sim 10^{18}$ $e\,\mathrm{cm}^{-2}$ at 7 MeV. E_0: incident electron energy. E_e: electron energy in sample. E_p: energy of displaced atoms. z: depth from the surface.

Theory (energy)	Experiment (temperature)	
(electron energy spectra) displaced atom energy	beam heat of sample (19 W/cm^2) + cooling	
collision with atom	displaced atom ($\sim 10^{18}$ cm^{-3})	bulk (5×10^{22} atoms cm^{-3})
$\langle n(E_0,z)$ Monte Carlo simulation $E_e=6.5$ MeV$\sim 0\rangle$	($\sim$100 eV) corresponds to very high temperature	20 °C (by cooling)
$N(E_p,z)$ Classical Coulomb scattering $E_p\approx 100$ eV~ 0	↓ migration	

$$\eta = dN/dx = n_0 \sigma \nu, \tag{8}$$

where N is the total number of displacements, n_0 is the number of atoms per unit volume, and σ and ν are a scattering cross section and a number of displaced atoms produced for each primary displacement, respectively. σ is given by

$$\sigma = \frac{\pi}{4} b'^2 \left(\left(\frac{E_m}{E_d} - 1 \right) - \beta^2 \ln \frac{E_m}{E_d} + \pi\alpha\beta \left\{ 2 \left[\left(\frac{E_m}{E_d} \right)^{1/2} - 1 \right] - \ln \frac{E_m}{E_d} \right\} \right), \tag{9}$$

where $\pi b'^2/4 = 2.495\times 10^{-25} Z^2/(\beta^4\gamma^2)$, $\gamma = 1/(1-\beta^2)^{1/2}$, and $\beta^2 = X(X+2)/(X+1)^2$. A displacement energy E_d of 25 eV (Ref. 29) was used in the calculation. In Fig. 4, a solid line shows the calculated concentration of displaced atoms at the surface as a function of electron energy for a Ge target. The energy dependences of SIMS intensity ratios are in fairly good agreement with that of the calculated concentrations of displaced atoms for Ge. In Fig. 6, a solid line shows the calculated concentration of displaced atoms as a function of electron energy for the sample of irradiated Zn. The energy dependence of the experimental results is in rough agreement with the calculated curve. These results also suggest that the EBD may be due to the displaced atoms produced by electron irradiation.

E. Enhanced diffusion

There are two kinds of interstitial-assisted diffusion processes. They are the Frank-Turnbull mechanism ($A_i + V \rightleftarrows A_s$) and the kick-out mechanism ($A_i \rightleftarrows A_s + I$), as shown in Fig. 12. In the unirradiated region, there is no vacancy, and a number of Ge interstitials exist. Such a condition is favorable for the kick-out mechanism. There may be diffusion enhancement under irradiation, which is a mixture of concentration-enhanced, mobility-enhanced, and correlation-enhanced diffusion. Under irradiation diffusion, enhancements by a factor of 10^6 or more can be achieved.[32]

1. Concentration-enhanced diffusion (kick out)

Concentration-enhanced diffusions may occur due to the high concentration layers of impurities at or near the surface. Near the surface of the substrate (layer 1) in the three-layer systems, Zn and Si concentrations are very high and the diffusivities D are relatively small (see Fig. 7). Since Zn and Si substitutional atoms have larger solubility and smaller D than Zn and Si interstitial atoms,[33] it is expected that most Zn and Si atoms are in the substitutional state there. This may be interpreted by considering the kick-out mechanism, originally proposed for Au in Si.[26] According to the mechanism, the following reactions occur:

$$\mathrm{Zn}_i \rightleftarrows \mathrm{Zn}_s + \mathrm{Ga}_i, \tag{10}$$

$$\mathrm{Si}_i \rightleftarrows \mathrm{Si}_s + \mathrm{Ga}_i, \tag{11}$$

where subscripts i and s represent interstitial and substitutional states, respectively. We can see from the law of mass action that the concentrations of Zn_s and Si_s are not high where a large number of Ga_i exist. During irradiation, many Frenkel pairs and thus Ga_i's are created, and therefore the Zn_s and Si_s concentrations will not be high in the bulk region. However, the Ga_i concentration is reduced near the surface since the surface acts as a sink of interstitials. Hence

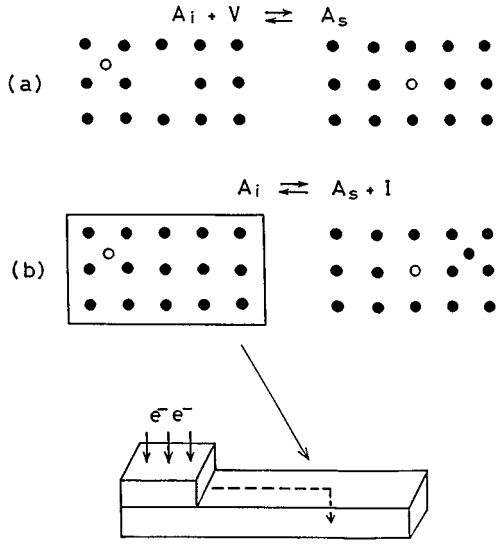

FIG. 12. The Frank-Turnbull (a) and the kick-out mechanisms (b) of interstitial diffusion. ○: initial interstitial atom; ●: original atoms sites.

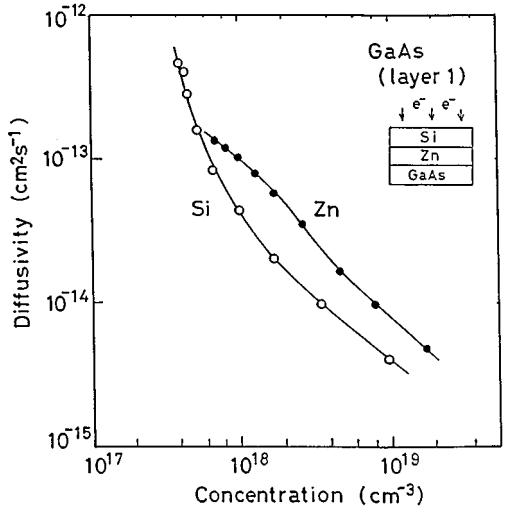

FIG. 13. Variation of diffusion coefficients of Zn and Si impurities in GaAs (layer 1) as a function of concentration calculated by the analysis of the Boltzmann and Matano method from the depth profiles of Zn and Si impurities measured by SIMS.

Zn_s and Si_s concentrations can be high near the surfaces. Also, fast surface diffusion and the kick-out mechanism will make the *U*-shaped diffusion Zn and Si profiles, as discussed in the previous paper.[6] Figure 13 indicates the Si and Zn concentration C dependences of the diffusivities $D(C)$, which were calculated by the analysis of Boltzmann and Matano from the depth profiles of impurities (see Fig. 7). The Zn and Si concentration C dependences of the diffusivities $D(C)$ are almost proportional to C^{-2}. This can be explained by taking account of the kick-out mechanism of Eqs. (10) and (11). The following reaction of the kick-out mechanism for Ga_i may be established via an As self-interstitial:[34]

$$Ga_i \rightleftarrows Ga_{As} + As_i , \tag{12}$$

The As_i concentration is reduced near the surfaces, since the surfaces may act as As_i sinks.

Thus, in the case of array III [Fig. 8(a)], PL signals attributed to Ga antisite defects Ga_{As} were observed before annealing. However, in the case of array II [Fig. 8(b)], the concentration of Ga_i created by the reaction of only Eq. (10) is much lower than that produced by both Eqs. (10) and (11) in array III. Then, in the two-layer system, a PL signal for Ga_{As} may disappear.

2. Mobility-enhanced diffusion

In semiconductors, if conduction electrons and/or holes recombine at, or are trapped by defects via nonradiative transitions, the defects may be displaced with the aid of the energy released in these processes.

We speculate that the strong enhancement of the diffusion will be due to the following energy release mechanism: when a carrier is nonradiatively captured at a defect (deep level), the phonons emitted help the defect to surmount potential barriers along the migration path. In the present experiments, excess carriers are generated by electron-beam irradiation, and simultaneously defects (e.g., vacancies and interstitial impurities) are also created. The defects will operate as traps or recombination centers for carriers, and their migration will be strongly activated.

The substrate dependence of alloying were studied for GaAs, GaSb, and GaP.[11] In Al/GaSb and Al/GaP systems, we confirmed the growth of alloy semiconductors even in the two-layer arrays (AII). Alloying in the Al/GaAs system, however, was rather difficult in the type-AII sample. Those results could be explained as follows: Phonons with a nonradiative recombination of electrons and holes play an important role in alloying of $Al_xGa_{1-x}P$ with an indirect-band-structure. GaSb has a direct-band structure with a low-energy separation (80 meV) between Γ and L valleys, and $Al_xGa_{1-x}Sb$ ($x>0.2$) has an indirect-band structure. Thus considerable electrons are distributed evenly in the L valley, and the rate of nonradiative recombination is larger than in $Al_xGa_{1-x}As$. On the other hand, $Al_xGa_{1-x}As$ has a direct-band structure with a large separation between Γ and L valleys; thus the excess carriers produced by electron irradiation will easily recombine radiatively. The energy escapes out of the crystal due to the formation of photons. Therefore, one can expect that alloying in the Al/GaP and Al/GaSb systems are easier than in the Al/GaAs system, and that the amount of alloyed Al increases in the order

$$GaAs < GaSb < GaP.$$

Also, the amount of Al incorporated into the substrate increases in the following order: Al/GaAs< $Al/GaAs_{1-y}P_y$<Al/GaP.[11] Defect reaction enhanced by nonradiative recombinations will become more frequent as P composition in the substrate increases. Thus if the nonradiative recombination plays some role in the EB epitaxy (EBE) process, the amount of the incorporated Al will increase with P composition.

The energy release mechanism has been theoretically discussed by Weeks, Tully, and Kimerling.[35] According to their model, the jump rate of a defect, k_d, is given by

$$K_d = R\frac{k^0}{k_{-1}}\left(\frac{E^*-\Delta E}{E^*}\right)^{s-1}\exp\left(-\frac{E^*-\Delta E}{kT}\right), \tag{13}$$

where R is the rate of capture (or recombination), E^* the migration enthalpy of the defect, ΔE the energy transferred to the defect on the carrier capture, S the number of modes of the vibration of the defect, and k_{-1} the rate of energy transfer from the defect to the surrounding lattice. k^0 is considered to be of the order of a vibration frequency (10^{13} sec^{-1}). As can be seen from this equation, the activation energy of the diffusion is reduced by ΔE owing to the energy release mechanism. D is calculated from k_d by

$$D = k_d d^2 g, \tag{14}$$

where d is the jump distance and g the geometrical factor.

Weeks, Tully, and Kimerling estimated k_{-1} to be 10^{13} sec^{-1}, and s to be 8.[35] R is the product of three terms as is Eq. (15), i.e., the capture cross section of defect σ, the carrier concentration n, and the thermal velocity v ($\sim 10^7$ cm sec^{-1} at room temperature),

$$R = n\sigma v . \tag{15}$$

The σ of traps in electron-beam-irradiated Si is measured as 10^{-12}–10^{-15} cm^2, and thus we tentatively assume here that $\sigma=10^{-14}$ cm^2.

The electron irradiation also produces high concentrations of electron-hole pairs (EHP's). The rate of generation G of electron-hole pairs per unit time by an incident electron can be estimated as follows:[36]

$$G=(1/\varepsilon)(dE/dx)(d\Phi/dt), \tag{16}$$

where ε is the energy for the formation of the EHP [$\sim$3.88 eV for Si, and $\sim$4.7 eV for GaAs (Ref. 37)], dE/dx the electron energy loss per cm of the path by a fast electron (3.9×10^6 eV cm^{-1} e^{-1} for Si, and 7.43×10^6 eV cm^{-1} e^{-1} for GaAs), and $d\Phi/dt$ the electron dose rate (3.7×10^{17} e cm^{-2} sec^{-1}). Assuming the above values, the irradiation results in $G\simeq3.7\times10^{23}$ and 5.5×10^{23} EHP's cm^{-3} sec^{-1} for Si and GaAs, respectively. In the steady state during the irradiation, n is given by

$$n=G\tau, \tag{17}$$

where τ is the carrier lifetime. The value of τ for the irradiated GaAs wafer was obtained as $\sim$2.7 ns. Then $n\simeq1.35\times10^{15}$ cm^{-3} for GaAs, and R becomes 10^8 sec^{-1}. ΔE would be about half of the band gap, i.e., 0.7 eV for GaAs. The migration enthalpies of the defects in GaAs has been obtained to be about 0.88 eV.[38] If $E^*-\Delta E$ (activation energy) is in the range of 0.1–0.2 eV, which agree with the experimental results, the value of D calculated from Eqs. (13) and (14) becomes 10^{-12}–10^{-15} cm^2 sec^{-1}, i.e., comparable to the experimentally determined values of D. Thus both the vacancy and interstitial states are considered to contribute to the observed enhanced diffusion.

F. *U*-shaped diffusion profile

U-shaped diffusion profiles of the impurities in the substrate were obtained experimentally by using secondary-ion-mass spectrometry (SIMS), as shown in Fig. 7. The results can be explained well by considering both the kick-out mechanism and surface diffusion process.[6]

So far the following outstanding feature of diffusion of Zn in GaAs have been established.[39] The diffusion of Si in GaAs is similar to one of Zn in GaAs. The Zn atom may occupy both substitutional (Zn_s) and interstitial (Zn_i) sites. The solubility of Zn_s is larger than that of Zn_i because the substitutional state is energetically favorable, whereas the diffusivity of Zn_i is much higher than that of Zn_s by several orders of magnitude. Thus the effective diffusivity of Zn atoms is not very large. The kick-out mechanism which was originally proposed for Au in Si (Ref. 40) is characterized by the generation of a Ga self-interstitial (Ga_i)

$$\mathrm{Zn}_i \underset{k_2}{\overset{k_1}{\rightleftarrows}} \mathrm{Zn}_s + \mathrm{Ga}_i\,, \tag{18}$$

where k_1 and k_2 are reaction constants, and subscripts i and s mean interstitial and substitutional states, respectively. Because of the high mobility of Zn_i, after a short time Zn_i has practically reached its solubility limit Zn_i^{eq} in the whole specimen. Considering the law of mass action of the kick-out reaction, we can see that the concentration of Zn_s is not high where a large number of Ga_i exists. During irradiation, many Frenkel pairs and thus Ga_i's are created, and therefore the Zn_s concentration will not be high in the bulk region. However, the Ga_i concentration is reduced near the surfaces since a surface acts as a sink of interstitials. Hence the Zn_s concentration can be high near the surfaces. This would give rise to a *U*-shaped diffusion profile.[6]

As shown in Fig. 7, the concentration is very high near the surface, while it is relatively low and almost constant in the bulk region except in the vicinity of the surfaces: i.e., the profiles are *U* shaped. The result of a computer calculation for the kick-out mechanism using Eq. (18) in a set of three partial differential equations was in qualitatively fair agreement with experimental diffusion profiles.[41]

G. Schematic diagram of a mechanism of EBD

The origin of electron-beam doping may be considered as follows.[30] First, electron irradiation of the impurity sheet on the substrate creates Frenkel defects and electron-hole pairs in the impurity sheet. There are a number of unrecombined interstitials in crystal, which are nearly equal to that of total observed vacancies. As the migration energy of interstitials is small (less than 0.22 eV for Si),[42] the interstitials migrate as an ''atomic beam'' owing to the energy transferred by recoil with electrons and displaced atoms, and they may sink at or near the surface. As a sticking probability of impurities at a wafer surface may be expected to be rather large from the experimental results of Fig. 9(b), the concentration of interstitials, reached at the surface, may increase under irradiation. The concentration of migrating interstitials becomes on the order of the matrix atoms. Surface diffusivities of impurities were on the order of 10^{10} times as large as the volume diffusivities.[16] Supersaturations of atoms at the surface may be built up, and some islands with impurities were introduced.[43] A small fraction of the monolayer of impurity atoms at or near the surface of the substrate may possibly be formed during irradiation. Thereby concentration-enhanced diffusions may be effected due to the high concentration of impurities at or near the surface. Furthermore, mobility-enhanced diffusion by recombination of electron-hole pairs with high concentrations produced by electron irradiations may also occur. Subsequently, the interstitials (impurity atoms) diffuse into the substrate from the impurity sheet by the above enhanced diffusions.

V. SUMMARY

The mechanism of electron-beam doping was studied experimentally and theoretically. The main results were obtained for the surface diffusion of foreign atoms, for the electron energy dependences of the doped-atom concentration, and for three-layer systems of Si/Zn/GaAs. The energy spectra of primary displaced atoms were calculated from the electron energy spectra computed by a Monte Carlo simulation. From the experiments, the surface diffusion of free-atom-like impurities was established, and its surface diffusivity was on the order of 10^{10} times as large as volume diffusivities. The electron energy dependences of the concentration for the doped atoms are in agreement with those calculated for the displaced atoms. These results suggest that the displaced atoms contribute to EBD. Subsequently, the mechanism of

EBD may be explained by the displaced atoms, the migration of them, surface diffusion with large diffusivities, a high concentration surface layer, and the concentration- and recombination-enhanced diffusions. Additionally, EBD processes would be useful or interesting, with advantages over alternative doping techniques, because even in the unirradiated region without damage and at room temperature, doping processes for shallow depths from the surface may be possible. Further studies will be carried out for the general problem of semiconductors, and the application of EBD.

ACKNOWLEDGMENTS

The authors wish to express their gratitude to M. Takeda and H. Masuda of the National Industrial Research Institute of Nagoya for their help in connection with bombardment of the sample and to Nissin-High Voltage Co. Ltd., for 750-keV electron irradiations by a Van de Graaf accelerator. This work was supported in part by the Scientific Research Grant-in-Aid from the Ministry of Education, Science, and Culture, the NEC Corporation, and the Chubu Electric Power Co., Inc.

[1] For example, J. W. Corbet, *Solid State Physics* (Academic, New York, 1966), Suppl. 7.
[2] B. A. Kulp and R. H. Kelley, J. Appl. Phys. **31**, 1057 (1960).
[3] J. H. Myer, J. Appl. Phys. **42**, 2851 (1971).
[4] T. Wada, in *Proceedings of the 3rd International Conference on Neutron Transmutation Doped Silicon, Copenhagen, 1981*, edited by Jens Guldberg (Plenum, New York, 1981), p. 447.
[5] T. Wada and M. Takeda, in *Proceedings of the 4th International Conference on Ion and Plasma Assisted Techniques, Kyoto, 1983*, edited by T. Takagi (Institute of Electrical Engineering of Japan, Tokyo, 1983).
[6] T. Wada and H. Hada, Phys. Rev. B **30**, 3384 (1984).
[7] T. Wada, M. Takeda, and K. Yasuda, J. Electron. Mater. **14**, 171 (1985).
[8] T. Wada and Y. Maeda, Appl. Phys. Lett. **51**, 2130 (1987).
[9] T. Wada, Appl. Phys. Lett. **52**, 1056 (1988).
[10] T. Wada and A. Takeda, Nucl. Instrum. Methods Phys. Res. Sect. B **37/38**, 352 (1989).
[11] T. Wada, Y. Maeda, and S. Kojima, Radiat. Eff. Defect Solids **111&112**, 471 (1989).
[12] T. Wada and Y. Maeda, Appl. Phys. Lett. **52**, 60 (1988).
[13] T. Wada, R. Abe, A. Takeda, M. Ichimura, and M. Takeda, Solid State Electron. **33**, 155 (1990).
[14] L. Boltzmann, Ann. Phys. **53**, 948 (1894).
[15] C. Matano, Jpn. J. Phys. **8**, 109 (1933).
[16] T. Wada, A. Takeda, M. Ichimura, and M. Takeda, in *Impurities, Defects, and Diffusion in Semiconductors: Bulk and Layered Structures*, edited by D. J. Wolford, J. Bernholc, and E. E. Heller, MRS Symposium Proceedings No. 163 (Materials Research Society, Pittsburgh, 1990), p. 549.
[17] T. Wada and E. Matsumoto, Inst. Phys. Conf. Ser. No. **59**, 347 (1981).
[18] P. W. Yu and D. C. Reynolds, J. Appl. Phys. **53**, 1263 (1982).
[19] K. R. Elliotl, D. E. Holmes, R. T. Chen, and C. C. Kirkpatric, Appl. Phys. Lett. **40**, 898 (1982).
[20] S. G. Bishop, B. V. Shanabrook, and W. L. Moore, J. Appl. Phys. **56**, 1785 (1984).
[21] T. Wada, A. Takeda, and M. Ichimura, in *Proceedings of the 15th International Conference on Defects in Semiconductors*, edited by G. Ferenczi (Trans Tech, Switzerland, 1989), p. 735.
[22] T. Wada, H. Fujimoto, and H. Masuda, in *Proceedings of the 18th International Conference on Defects in Semiconductors*, edited by K. Sumino, Materials Science Forum (Trans Tech, Switzerland, in press).
[23] J. S. Savdejas and J. B. Hudson, in *Fundamentals of Gas-Surface Interaction*, edited by H. Saltsburg, J. N. Smith, and M. Rogers (Academic, New York, 1967), p. 271.
[24] L. Pauling, *The Nature of the Chemical Bond*, 3rd ed. (Cornell University Press, Ithaca, NY, 1960),
[25] J. H. Cahn, J. Appl. Phys. **30**, 1310 (1959).
[26] U. Gosele, W. Frank, and A. Seeger, Appl. Phys. Lett. **23**, 361 (1981).
[27] H. Sugiyama, Bull. Electrotech. Lab. **34**, 577 (1970).
[28] S. K. Anderson, F. Bell, F. Frandsen, and E. Uggerhoj, Phys. Rev. B **8**, 4913 (1973).
[29] E. G. Wikner, Phys. Rev. **138**, A294 (1965).
[30] K. Yasuda and T. Wada, Jpn. J. Appl. Phys. **33**, 3622 (1994).
[31] J. Ishikawa, Y. Takeiri, K. Ogawa, and T. Takagi, J. Appl. Phys. **61**, 2509 (1987).
[32] B. J. Masters and E. F. Gorey, J. Appl. Phys. **49**, 2717 (1978).
[33] L. R. Weisberg and J. Blanc, Phys. Rev. **131**, 1548 (1963).
[34] U. Gosele, F. Morehead, W. Frank, and A. Seeger, Appl. Phys. Lett. **38**, 157 (1981).
[35] J. D. Weeks, J. C. Tully, and L. C. Kimerling, Phys. Rev. B **12**, 3286 (1975).
[36] J. C. Bourgoin and J. W. Corbett, Radiat. Eff. **36**, 157 (1978).
[37] E. Baldinger, W. Czaja, and A. Z. Farooqi, Helv. Phys. Acta. **33**, 551 (1960).
[38] H. Sumi, Phys. Rev. B **29**, 4616 (1984).
[39] C. H. Ting and G. L. Person, J. Electrochem. Soc. **118**, 454 (1971).
[40] W. Frank, A. Seeger, and U. Gosele, *Defects in Semiconductors* (North Holland, Amsterdam, 1981), p. 31.
[41] A. Takeda and T. Wada, Mater. Sci. Forum **143–147**, 1421 (1993).
[42] R. R. Hasiguti, J. Phys. Soc. Jpn. **21**, 1927 (1966).
[43] T. Wada, H. Fujimoto, and H. Masuda, in *Proceedings of the 18th International Conference on Defects in Semiconductors* (Ref. 22).